*Journal of Superconductivity: Incorporating Novel Magnetism, Vol. 15, No. 1, February 2002 (© 2002)*

# Diluted Magnetic Semiconductors in the Low Carrier Density Regime

**R. N. Bhatt,[1,2,3] Mona Berciu,[2] Malcolm P. Kennett,[3] and Xin Wan[4]**

*Received 26 November 2001*

This paper, based on a presentation at the Spintronics 2001 conference, provides a review of our studies on II–VI and III–V Mn-doped Diluted Magnetic Semiconductors. We use simple models appropriate for the low carrier density (insulating) regime, although we believe that some of the unusual features of the magnetization curves should qualitatively be present at larger dopings (metallic regime) as well. Positional disorder of the magnetic impurities inside the host semiconductor is shown to have observable consequences for the shape of the magnetization curve. Below the critical temperature the magnetization is spatially inhomogeneous, leading to very unusual temperature dependence of the average magnetization as well as specific heat. Disorder is also found to enhance the ferromagnetic transition temperature. Unusual spin and charge transport is implied.

**KEY WORDS:** diluted magnetic semiconductors; disorder; magnetism; metal-insulator transition.

## 1. INTRODUCTION

Diluted magnetic semiconductors (DMS) are composed of an inert host semiconductor doped with both localized spins and carriers (electrons or holes) that are either itinerant, or localized on a much longer length scale. In that sense, they belong to the general family of correlated electron systems, which include a number of fascinating materials such as cuprates, manganites, heavy fermions, and other Kondo lattice systems.

Electronic materials containing local moments have been studied for some time. What makes the DMS so fascinating is that they belong to a regime that has previously been neglected. While the name diluted magnetic semiconductors implies (correctly) that the system has only a small percentage of localized spins, they are at the opposite extreme of the dilute magnetic alloys such as Fe or Mn in Cu, the canonical systems involving itinerant fermion and localized spin degrees of freedom, which have been studied extensively [1]. In the dilute magnetic metallic alloys, the low density of spins are a perturbation on the Fermi liquid representing the nonmagnetic host metal, so depending on the concentration of the local moments, they may be studied in terms of dilute Kondo systems, or amorphous magnetic systems with a spin–spin coupling mediated by the Fermi sea of conduction electrons (RKKY coupling), which lead often to spin glass behavior [2].

By contrast, in the regime of interest, the carrier density in DMS is significantly *lower* than the (low) localized moment density, so the spins become an integral part of the description of the system and its magnetic phase, rather than a mere perturbation on a metallic Fermi sea. In that sense, the situation is even more extreme than e.g., in Kondo lattice and Heavy Fermion materials, where the two species have comparable densities. This large, inverted, ratio of local moments to carriers is in fact similar to that in the high $T_c$ cuprates. However, unlike the cuprates, the density of local moments is low and incommensurate with the lattice, and the carriers and the spins are not in the same band. As a consequence of the low moment

[1]Department of Electrical Engineering, Princeton University, Princeton, New Jersey 08544.
[2]Princeton Materials Institute, Princeton University, Princeton, New Jersy 08544.
[3]Department of Physics, Princeton University, Princeton, New Jersey 08544.
[4]National High Magnetic Field Laboratory and Department of Physics, Florida State University, Tallahassee, Florida 32306.



0896-1107/02/0200-0071/0 © 2002 Plenum Publishing Corporation

density, the exchange between local moments is not standard direct or superexchange, as in the cuprates, but is mediated by the carriers, even though their density is so small. Thus, the DMS are in rather different region of phase space of electronic materials with local moments, than other correlated electron systems.

Despite this difference, most models of diluted magnetic semiconductors start from the high carrier density limit, where the carriers may be modeled as free carriers moving in the conduction or valence band [3]. This is understandable, since in the high density limit the carrier kinetic energy is the largest energy in the problem, and calculations may be done perturbatively starting from the noninteracting Fermi gas. However, most of the interesting behavior is seen at low carrier densities, where the system is insulating, or not too far from the metal-insulator transition. Consequently, we have concentrated in this work on the low density regime, starting from bound carriers, and moving on to carriers in an impurity band formed from the bound impurity states.

As we wish to cover the case of insulating behavior at arbitrary filling factor i.e., away from the half filled impurity band case (one carrier per site), disorder has to be included at the outset. In particular, we model the system with randomly distributed dopants, as in the experimental system, since it has been recognized that the random distribution is essential to understand the magnetic properties of conventional, nonmagnetic doped semiconductors [4,5]. Such models exhibit both insulating and metallic phases, and with the random distribution of impurity sites included, are in a position to reveal the effect of disorder in low carrier density systems. In the case of the predominantly antiferromagnetic couplings between hydrogenic centers in conventional doped semiconductors, the randomness is found to suppress magnetic order below measurable temperatures (∼millikelvin), and possibly to zero. In the case of DMS, where interactions lead to ferromagnetic ordering [6,7], in agreement with experimental findings [8,9], we find that randomness leads to unusual behavior in the magnetic response, and effects of randomness are expected in the transport behavior as well.

In this paper, we review the results of our approach to DMS based on both II–VI semiconductors (like CdTe or ZnSe), and on III–V semiconductors (such as GaAs or GaP; for a review of properties of ferromagnetic III–V semiconductors, see Ref. [9]), and compare the two families of DMS systems. The paper is organized as follows. In Section 2 we briefly review the properties of conventional (insulating) ferromagnets. The results presented serve as a reference with which to contrast the results obtained in the rest of the paper. Section 3 addresses the II–VI based DMS, while Section 4 deals with III–V DMS. In each case, we introduce the Hamiltonians we use to model these systems. Results obtained within mean-field approximation (MFA) and with Monte Carlo (MC) simulations are presented. The effect of positional disorder of the Mn dopants is studied, as are the similarities and differences between II–VI and III–V DMS. Finally, Section 5 summarizes our results and conclusions. It also includes a discussion of important issues such as robustness of models, relevance of disorder on spin scattering, and key experiments which could help provide a better understanding of these materials.

## 2. CONVENTIONAL FERROMAGNETIC SYSTEMS

A typical model of a uniform ferromagnet consists of a collection of identical magnetic spins of magnitude $S$, placed on an ordered Bravais lattice. While the generic case may be anisotropic in spin space due to a variety of reasons (spin–orbit coupling, crystal fields etc.) we consider here the simplest isotropic case where the spin interactions are well described by a Heisenberg Hamiltonian

$$\mathcal{H} = -\sum_{i \neq j} J_{ij} \vec{S}_i \cdot \vec{S}_j - \vec{H} \cdot \sum_i g\mu_B \vec{S}_i. \qquad (1)$$

Because of translational invariance, the exchange integral $J_{ij}$ depends only on the distance $\vec{R}_i - \vec{R}_j$ between spins. In insulating materials, this dependence is due to overlap between the electronic orbitals involved in creating the spin $S$ (through Hund's rule), leading to an exponential decay of $J_{ij}$ with increasing distance. In typical magnetic atoms, these orbitals are of d or f type, and they are localized within ∼1–2 Å of the nucleus. As a result, it is customary to restrict the first sum in Eq. (1) to only nearest-neighbor spins. The external magnetic field $\vec{H} = H\hat{e}_z$ breaks the rotational symmetry, leading to the appearance of a nonvanishing expectation value $\langle S_i^z \rangle$ at each site. Translational invariance implies that $\langle S_i^z \rangle = \langle S \rangle$ is independent of the position $\vec{R}_i$ of the spin.

While an exact solution for the Heisenberg Hamiltonian (1) is known only in one dimension, it has been found that the Weiss (mean-field) approximation provides a qualitatively good understanding of the properties of these systems. The

mean-field factorization $\vec{S}_i \cdot \vec{S}_j \to \vec{S}_i \cdot \langle \vec{S}_j \rangle + \langle \vec{S}_i \rangle \cdot \vec{S}_j - \langle \vec{S}_i \rangle \cdot \langle \vec{S}_j \rangle = \langle S \rangle (S_i^z + S_j^z) - \langle S \rangle^2$ allows for a solution of the problem in terms of an effective magnetic field $H(i) = H + J\langle S \rangle / (g\mu_B)$, where $J = \sum_{j \neq i} J_{ij}$. (If only nearest-neighbor interactions are kept, $J = zJ_{01}$, where $z$ is the coordination number of the Bravais lattice and $J_{01}$ is the exchange integral for nearest-neighbor spins.) In the absence of an external magnetic field, a nonvanishing solution for $\langle S \rangle$ is found for $T \leq T_C = JS(S+1)/3k_B$. In other words, the system is ferromagnetically aligned below the critical temperature $T_C$, and the spontaneous magnetization $\langle M \rangle = g\mu_B \langle S_i^z \rangle$ increases rapidly (Fig. 1) with decreasing temperature and is already close to the saturation value $M_0 = g\mu_B S$ below $T < 0.5T_C$. Concurrently, the specific heat has a peaked structure around $T_C$ and drops rapidly to zero for $T < 0.5T_C$ reflecting the fact that the only accessible degrees of freedom for low $T$ are the long-wavelength (collective) spin-wave excitations which have a restricted phase space (see Fig. 2) [10].

It is well-known that MFAs overestimate the strength of the correlations, leading to rather high estimates for the Curie temperatures $T_C$. Detailed studies of these Hamiltonians with Monte Carlo simulations, which properly account for the effects of thermal fluctuations, find quantitative changes of up to a factor of 2 in the value of $T_C$. However, as suggested in Fig. 2,

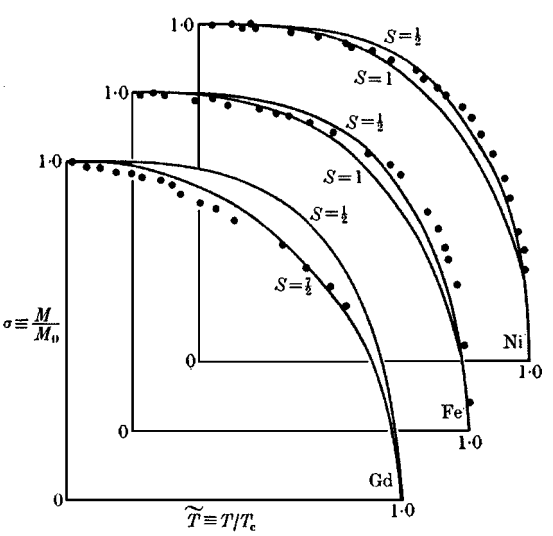


**Fig. 1.** Dependence of reduced magnetization $M/M_0$ upon reduced temperature $T/T_C$. Curves are slightly different for different values of the quantum spin $S$, however they all have a convex upward shape. The solid circles represent typical experimental data for Gd ($S \approx \frac{7}{2}$), Fe ($S \approx 1$), and Ni ($S \approx \frac{1}{2}$) (From Ref. [10]).

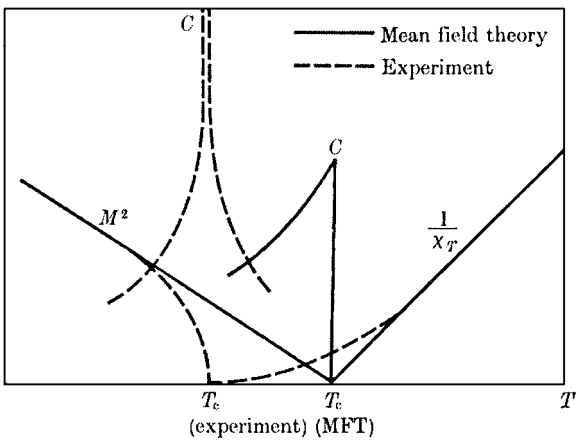


**Fig. 2.** Schematic comparison of typical experimental measurements of temperature dependence of magnetization, specific heat and susceptibility for a Heisenberg ferromagnet (such as EuS) with the predictions of the Weiss mean-field theory. Note that the curve for inverse susceptibility $1/\chi_T$ is shown only for $T > T_C$ (From Ref. [10]).

the *qualitative* features of the magnetization, specific heat, and susceptibility curves remain as in the Weiss mean-field treatment, in good agreement with experimental measurements.

## 3. FERROMAGNETIC SYSTEMS: II–VI DMS

### 3.1. The Model

The II–VI DMS are based on semiconductors AB, where A is a group-II element and B is a group-VI element (such as CdTe or ZnSe). In the II–VI DMS, some of the divalent sites (Cd/Zn) are substituted by a magnetic element, typically Mn. This fraction is denoted by $x$, so the DMS we consider is $A_{1-x}Mn_xB$. Mn is also a group-II element, but in addition it has a half-filled 3d shell, with a total spin given by Hund's rule: $S = 5/2$. In the absence of other types of dopants, the system $A_{1-x}Mn_xB$ is an insulator which exhibits antiferromagnetic (AFM) tendencies at low temperatures. This is seen, for instance, from measurements of the susceptibility which is found to depend on temperature as $\chi(T) \sim 1/(T + T_N)$, with a Neel temperature of a few kelvin [8,11]. The origin of this AFM tendency is the (expected) antiferromagnetic exchange between the Mn spins. However, for low doping concentrations $x$, the average distance between Mn spins is large and this AFM direct exchange is rather small.

When a low density of charged dopants, such as group-V Phosphorus (P) substituting for the group-VI

element, is introduced in the system, each of them binds a hole (or electron) in a shallow hydrogenic 1s state $\phi(\vec{r}) \sim \exp(-r/a_B)$, characterized by a Bohr radius $a_B \sim 10$–$20$ Å. Exchange interactions arise between the spins of these charge carriers and the Mn spins, and are described by the Hamiltonian [6].

$$H = \sum_{i,j} J(\vec{r}_i, \vec{R}_j)\vec{s}_i \cdot \vec{S}_j. \quad (2)$$

Here, $\vec{S}_j$ is the spin of the Mn at position $\vec{R}_j$ and $\vec{s}_i$ is the spin of the electron/hole centered at $\vec{r}_i$. The exchange interaction $J(\vec{r}_i, \vec{R}_j)$ is dependent on the overlap between the orbital $\phi(\vec{r} - \vec{r}_i)$ of the charge carrier and the orbitals $\psi_d(\vec{r} - \vec{R}_j)$ of the 3d electrons responsible for the Mn spin. Since these 3d orbitals are localized on a scale of a few Å around the Mn nucleus, the exchange is proportional to the carrier charge density at the Mn site, i.e.

$$J(\mathbf{r}_i, \mathbf{R}_j) = J_0|\phi(\vec{R}_j - \vec{r}_i)|^2 = J_0\, e^{-2|\mathbf{r}_i - \mathbf{R}_j|/a_B}, \quad (3)$$

where $J_0$ characterizes the strength of the exchange. Typically, for electrons $J_0 < 0$, while for holes $J_0 > 0$. However, since in the following we treat the spins as classical variables, the sign is irrelevant. For specificity, in the rest of the paper we assume $J_0 > 0$ corresponding to holes as charge carriers.

The Hamiltonian (2) neglects the direct AFM interactions between the Mn spins. For low values of the fraction $x$, it can be simply accounted for in the following manner. For Mn spins which are very close to one another (such as nearest neighbors), the direct AFM exchange is the dominant (large) interaction, and leads to the formation of a singlet state. This singlet becomes inert as far as magnetic interactions are concerned. For Mn spins which are fairly far apart from other Mn spins, the dominant magnetic interaction is the exchange with the charge carrier spins. As a result, to first order the Hamiltonian (2) accounts for both types of interactions if we restrict the summation over the Mn spins to only those Mn spins which are not part of a spin-singlet. At low $x$, this includes a large majority of Mn spins. If the fraction $x$ of Mn becomes too large, both types of interactions will be of comparable size for all the Mn spins, and therefore this separation is no longer possible. In this case, the frustration imposed by the competing exchanges leads to the appearance of a spin glass state, which has been observed experimentally for $x \geq 0.2$ [12]. In the following, we restrict ourselves to the low $x$ ($x \leq 0.1$) limit.

Simple thermodynamic considerations show that, qualitatively, at a temperature $k_B T < J(r)$ (see Eq. (3)), all Mn spins within distance $r_T \sim (a_B/2)\ln(J_0/k_B T)$ of a dopant order their spins antiferromagnetically with respect to the dopant hole spin. As a result, a region with a large magnetization (from all the parallel polarized Mn spins) appears near the dopant. This is known as a Bound Magnetic Polaron (BMP) [8], whose radius $r_T$ (see above) increases logarithmically with decreasing temperature. As a result, one expects that long-range ferromagnetic order appears in the system for temperatures low enough that a continuous percolating network of BMPs is formed (as shown schematically in Fig. 3), provided that nearby BMPs prefer to orient ferromagnetically with respect to one another. At first sight, this seems to not be the case, since direct exchange between the charge carriers localized in hydrogenic orbitals has an AFM sign [4,5,13]. However, this AFM coupling is overwhelmed by effectively ferromagnetic interactions between BMPs coming in part from Mn spins in between the polarons which favor ferromagnetic alignment of Mn spins [6] and partly from the modification of the effective direct exchange as a result of the local field due to the polarized Mn [7].

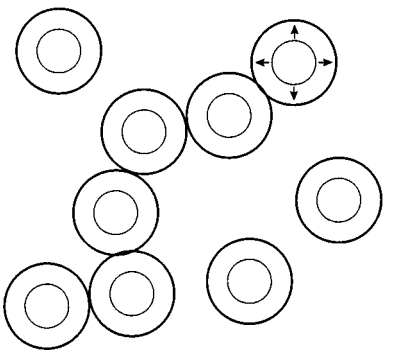

**Fig. 3.** Schematic drawing of the percolation limit for a disordered collection of BMPs. As the temperature is lowered, the size of each BMP increases and a percolated network appears below $T_C$. Just below $T_C$, only a small fraction of the spins belong to the percolated network and sustain the bulk magnetization of the sample. The large majority of spins is outside the percolated network and behave like quasi-free (noninteracting) spins.

These mechanisms favoring parallel orientation of the BMPs at low temperatures are rather weak, and as a result the Curie temperature below which long-range ferromagnetism is observed in these systems is very low, to our knowledge below 5 K for all II–VI DMS studied so far. Moreover, as the transition is of a percolation type, and the percolation fraction is ~20% for three dimensions, this implies that just below $T_C$ about 80% of the Mn spins do not participate in the ferromagnetism. These are the Mn spins which are outside the percolated cluster,

i.e., far from the charged dopants (see Fig. 3). They are very weakly interacting (essentially disordered) unless the temperature becomes so low that a nearby BMPs grows large enough to include them. This results in a very unusual FM phase, in which a substantial part of the spin entropy survives down to very low $T$.

### 3.2. Monte Carlo Simulations

We performed MC simulations on the Hamiltonian (2), to study this unusual FM phase, treating both Mn and carrier spins as classical variables [14]. This appears to be a reasonable approximation, since $S = 5/2$ is a large spin and the Mn spins dominate the magnetic response. Simulations were carried out for zinc-blende lattices with lattice constant $a = 5$ Å, for Mn concentration $x = 0.001$, dopant density $n_d = 10^{18}$ cm$^{-3}$ and $a_B = 20$ Å. The exchange $J_0$ defines the unit of energy. With these parameters, the Mn concentration $n_{Mn} = 4x/a^3$ is 32 times the dopant concentration. Nevertheless, the magnetic coupling is mediated by the latter because of the large Bohr radius, as required for the polaron picture to hold.

The magnetization curves obtained have unusual, concave upward shapes (see Fig. 4, left panel), very unlike the typical magnetization curve of Fig. 1. For these parameters, the critical temperature $T_C = 0.014J_0$ is found using finite size scaling [14]. We find that the magnetization reaches its saturation value only at exponentially small temperatures, reflecting

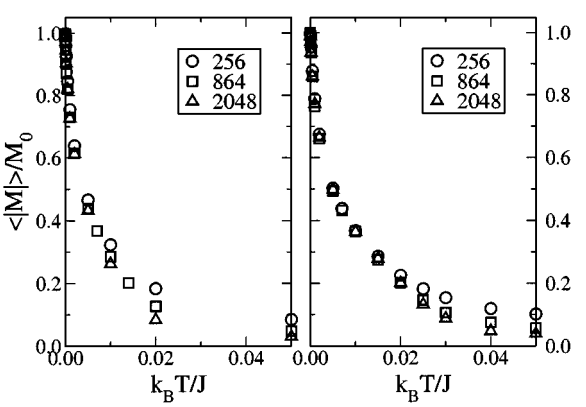


**Fig. 4.** Magnetization per Mn spin as a function of temperature, in a II–VI DMS, for classical/discrete spin model (left/right panel). Results are shown for samples with $N = 256$, 864, and 2048 Mn spins. Finite size scaling analysis finds a critical temperature $T_C = 0.014J_0$ [14]. The magnetization curves are very unlike the conventional ferromagnet magnetization curve shown in Fig. 1.

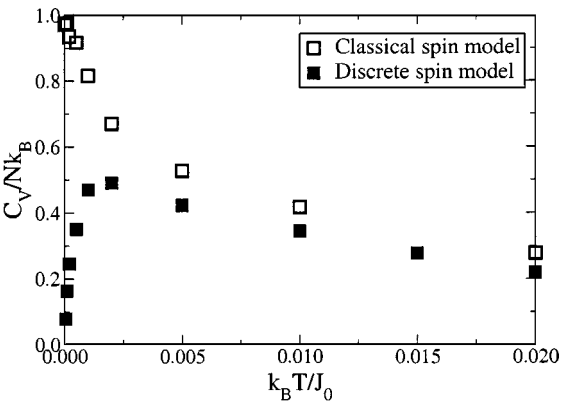


**Fig. 5.** Specific heat per Mn spin as a function of temperature, for classical (empty squares) and discrete (full squares) spin models. Systems with $N = 2048$ Mn spins were used in both cases. While the discrete model recaptures the proper limit $C_V \to 0$ as $T \to 0$, the peak in the specific heat is well below the critical temperature ($T_C = 0.014J_0$ for these parameters), unlike in conventional ferromagnets, where the peak in the specific heat is at $T_C$ (see Fig. 2).

the existence of the quasi-free Mn spins outside the percolated (magnetically ordered) region.

The specific heat of the classical Heisenberg model has the unphysical limit $C_V \to Nk_B$ as $T \to 0$ (empty squares in Fig. 5). While this agrees with the equipartition theorem, it implies that quantum mechanics (with discrete energy levels) is needed to capture the correct limit $C_V \to 0$ as $T \to 0$. One way to mimic the discretization, but avoid the complexities of the quantum MC treatment, is to use a discrete (classical) vector model, in which each Mn spin can only be oriented along one of the six (100) directions. An efficient MC method for this discrete model is described in Ref. [14]. While the magnetization curves are very similar to the ones obtained in the continuous spin Heisenberg model (see Fig. 4), the specific heat results are very different (see Fig. 5). As expected, for the discrete model $C_V \to 0$ as $T \to 0$. However, unlike in the case of a typical FM, the peak in $C_V$ is not near $T_C$, but at temperatures well below $T_C$. This reflects the residual entropy of the free Mn spins outside the percolated region.

### 3.3. Effect of Disorder

In II–VI DMS there are two sources of positional disorder: disorder in the positions of the Mn spins and disorder in the position of the charged dopants. In the limit when there are many Mn ions per dopant, the Mn spin disorder is not expected to have a significant effect on the magnetization curves, or the critical

temperature. The reason is that at the very low temperatures where percolation appears, the radius of each BMP is significantly larger than $a_B$, favoring interactions with a large number of Mn spins. Disorder in the Mn positions will lead to some fluctuations in the average number of Mn spins found in each BMP, but this should have a relatively small effect.

On the other hand, disorder in the position of the charged carriers (centers of the BMPs) has a large effect on the critical temperatures. As seen from Fig. 3, disorder in the positions of the BMPs facilitates the appearance of a large percolated cluster for smaller BMPs sizes (larger temperatures), since only a subset of the BMPs must percolate in order for ferromagnetic order to appear in the system. On the other hand, the ordered BMP lattice only percolates when each and every BMP is included. This obviously happens when a larger fraction of the space is filled by BMPs, i.e., at a lower temperature. However, we emphasize again that even for the ordered BMP lattice, a significant volume containing a large fraction of the Mn spins is still outside the percolated volume (in the interstitial spaces) and therefore the phenomenology related to the existence of weakly interacting spins down to exponentially low temperatures is still valid.

We have verified, using MC simulations, that the critical temperature of a system in which the charge carriers are placed in an ordered superlattice is lower than that of a sample with random positions of the charge carriers, when all other parameters are identical. For the case investigated, the relative increase of $T_C$ with disorder was 50% [15]. However, this relative increase is expected to depend on the various parameters of the problem.

## 4. FERROMAGNETIC SYSTEMS COUPLED TO FERMIONS: III–V DMS

### 4.1. Introduction

When Mn is doped in a III–V semiconductor, such as GaAs, the major difference with respect to the II–VI DMS is that the Mn atom provides both the $S = 5/2$ spin and the dopant charge carrier (a hole, since divalent Mn substitutes for trivalent Ga). While this implies nominally equal concentrations of holes and Mn spins, experimentally it is found that the hole concentration is only $p = 10$–$30\%$ of the Mn concentration [9,16]. The compensation process(es) responsible for the removal of such a large fraction ($\sim$70–90%) of the holes from the carrier band are not fully understood, but it is believed that an important role is played by As antisite defects. Such defects are created when group-V As substitutes for group-III Ga, and removes two holes introduced by Mn impurities, thus effectively decreasing the hole concentration. Compensation is responsible not only for the substantial decrease of the hole concentration, but also leads to the appearance of charged compensation centers (e.g. $As^{2+}$ for As antisites). The Coulomb potential created by these charged compensation centers may also play a role in the physics of these systems, as we discuss in the following.

As in the (II,Mn)VI systems, the main magnetic interaction in the (III,Mn)V DMS is the exchange between the Mn spins and the hole spins, which is known to be AFM [9]. Assuming, again, very sharply peaked Mn 3d orbitals, this exchange is proportional to the probability of finding the charge carrier at the Mn site. This probability is extracted from the wave-functions of the orbitals occupied by the hole charge carriers. The appropriate framework to describe the hole states depends on their concentration. At low hole concentrations, screening processes are ineffective. The unscreened Coulomb potentials of the Mn dopants are responsible for the splitting of hydrogen-like impurity levels from the top of the valence band, and the holes occupy these impurity states. In the limit of high hole concentrations when the carrier kinetic energy is the largest energy in the problem, the Coulomb potential of the Mn dopants effectively gets reduced because of screening. As a result, the holes occupy a Fermi sea at the top of the valence band. Qualitatively, it is apparent that the two situations could lead to quite different physics. Holes occupying Bloch states in the valence band are found with equal probability anywhere inside the host semiconductor, and therefore one expects the system to be rather homogeneous. On the other hand, holes occupying impurity states are found with high probability near the Mn sites. As a result, we expect a rather inhomogeneous distribution of the holes in the host semiconductor, and the positional disorder of the Mn dopants may play an important role, since it defines the length-scale for these inhomogeneities.

$Ga_{1-x}Mn_xAs$ has a metal-insulator transition for $x \sim 0.03$ and shows reentrant insulating behavior for $x > 0.07$ [9]. In the insulating regimes, the low-temperature conductivity is consistent with Mott long-range variable hopping [16,17], suggesting the existence of impurity-like levels. Even for the most metallic sample ($x = 0.053$) the screening length ($l \sim 10$ Å) as evaluated from the Thomas–Fermi theory is

of comparable size, not much smaller than the Bohr radius of the impurity level ($a_B \sim 8$ Å) [18,19].

### 4.2. The Model

Motivated by these observations, we have attempted to understand the low $x$ regime within a model based on the existence of impurity hydrogen-like orbitals at each Mn site. While this is similar to our approach to the II–VI DMS systems, one difference is that since the number of holes is smaller than the number of Mn, there must be a mechanism to allow the holes to "choose" the Mn dopants near which to stay. Such a mechanism is naturally provided by hopping processes facilitated by the overlap between impurity wave-functions centered at different Mn sites. Therefore, the Hamiltonian describing such a system is of the form

$$\mathcal{H} = \sum_{i,j} t_{ij} c^\dagger_{i\sigma} c_{j\sigma} + \sum_i [u(i) c^\dagger_{i\sigma} c_{i\sigma} + U n_{i\uparrow} n_{i\downarrow}] + \sum_{i,j} J_{ij} \vec{s}_i \cdot \vec{S}(j) + \sum_{i,j} K_{ij} \vec{S}(i) \cdot \vec{S}(j) - g\mu_B H \sum_i \frac{\sigma}{2} c^\dagger_{i\sigma} c_{i\sigma} - \tilde{g}\mu_B H \sum_i S^z(i). \quad (4)$$

Here, $i$ indexes different Mn positions $\mathbf{R}_i$, and $c^\dagger_{i\sigma}$ is the creation operator for a hole with spin $\sigma$ in the impurity level centered at $\mathbf{R}_i$, while $\vec{S}_i$ is the spin of the corresponding Mn dopant.

The first line in Eq. (4) is the Hamiltonian of the charge carriers. The first term describes hopping of holes between impurity levels. For simplicity, we assume again 1s impurity states with $\phi(\vec{r}) = \exp(-r/a_B)$. In fact, the hole impurity wave-function is more complicated, because of the band-structure of the valence band from which it splits (for details, see Ref. [18]). For the hopping integral we use the simple parameterization $t_{ij} = 2(1 + r/a_B)\exp(-r/a_B)$ Ry, where $r = |\mathbf{R}_i - \mathbf{R}_j|$, appropriate for hopping between two isolated 1s impurities which are not too close to one another [20]. For Mn doped into GaAs, the Bohr radius is $a_B = 7.8$ Å and the binding energy which defines the Rydberg is 1 Ry = 110 meV [18,19]. We have investigated other parameterizations for the hopping matrix $t(r)$ elsewhere [21], and found that while they lead to quantitative changes, qualitatively the results are similar.

The second term describes an on-site potential $u(i)$ due to the Coulomb potential of the other Mn impurities, as well as other nearby charged compensation centers. An on-site Coulomb repulsion $U$ of the Hubbard type may be added to describe the electron–electron repulsion between electrons occupying the same impurity orbitals. For isolated 1s impurities, $U \approx 1$ Ry. However, depending on the effectiveness of screening, the electron–electron interactions may be longer-range. A fully self-consistent treatment of this problem should involve a proper description of the screening processes, and would allow a detailed computation of the strength of the hopping matrix, the on-site Coulomb potential and the electron–electron interactions. However, since the full self-consistent description is extremely difficult to achieve, especially as details about compensation processes are still not clarified, we use the simplified assumptions described above. We believe that they should provide a good qualitative description of the properties of these compounds, and with proper fitting of various energy and length scales may even lead to a quantitative description.

The second line of Hamiltonian (4) describes the AFM exchange between the Mn spin $\vec{S}(j)$ and the hole spin $\vec{s}_i = \frac{1}{2} c^\dagger_{i\alpha} \vec{\sigma}_{\alpha\beta} c_{i\beta}$ ($\vec{\sigma}$ are the Pauli spin matrices). As in II–VI DMS, the AFM exchange is proportional to the probability of finding the hole trapped at $\vec{R}_i$ near the Mn spin at $\vec{R}_j$, so $J_{ij} = J\exp(-2|\vec{R}_i - \vec{R}_j|/a_B)$. Based on calculations [18] of the isolated Mn impurity in GaAs, we estimate the exchange coupling between a hole and the trapping Mn ($\vec{R}_i = \vec{R}_j$) to be $J = 15$ meV.

The second term describes the direct Mn–Mn exchange in the semiconductor host, which is expected to be short range, and consequently not important at low $x$ when Mn are a few sites away from each other. We have therefore omitted this term (i.e., set $K_{ij} = 0$); however, for higher concentrations this may be important. Finally, the third line in Hamiltonian (4) describes the interaction with an external magnetic field.

Given the large number of terms in the Hamiltonian, it is useful to try to understand the effect of each. To begin with, we neglect the random on-site potential ($u(i) = 0$), the electron–electron interaction ($U = 0$), the direct Mn–Mn AFM interactions ($K_{ij} = 0$) and turn off the external magnetic field ($H = 0$) (we will discuss the effects of these various terms later on). As a result, the Hamiltonian contains only its two main terms ($t_{ij}$ and $J_{ij}$), describing the dynamics of the charge carriers and the AFM interaction between the Mn spins and the charge carrier spins.

### 4.3. Similarities and Differences Between II–VI and III–V DMS

We investigated the Hamiltonian (4) using both the MFA [19,21] and MC simulations [22]. Typical magnetization curves obtained with MC methods for a Mn concentration $x = 0.01$ and hole concentrations $p = 10$ and 30% are shown in Fig. 6. The corresponding curves obtained using the MFA for the similar parameters are shown in Fig. 7. While there are substantial quantitative differences between the two, these are easily understandable. The long tail of the MC curves at high $T$ are due to finite sizes of the samples studied; these disappear as the sample size is increased. On the other hand, the critical temperature ($T_C$) predicted by MFT are significantly higher than those obtained by MC simulations (as would be expected). Part of the difference in $T_C$ between the two methods is actually due to the fact that the Mn spins in the MC simulations are taken to be classical variables, and quantum operators in the MFA. If we use classical Mn spins in MFA, we find $T_C$ reduced by a factor of ∼2. The remaining reduction is presumably due to the usual neglect of fluctuations in MFA, which is properly captured in MC simulations.

The striking feature, common to both results, is that the magnetization curves have unusual shapes—linear or concave upward. This is qualitatively similar to those found for the II–VI DMS (Fig. 4), and what has been seen in experiments [16,23], but very different from the convex upward $M(T)$ of conventional ferromagnets (Fig. 1). Again, as in the II–VI, the

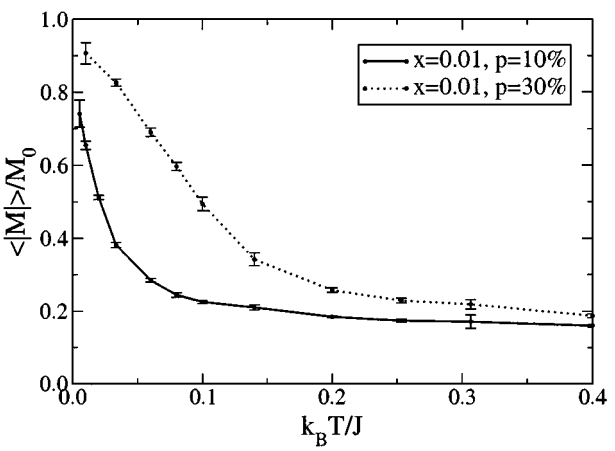


**Fig. 6.** Magnetization per Mn spin as a function of temperature, in a III–V DMS, using Monte Carlo simulations [22]. Curves correspond to $x = 0.01$, and relative hole to Mn concentrations $p = 10$ and 30%.

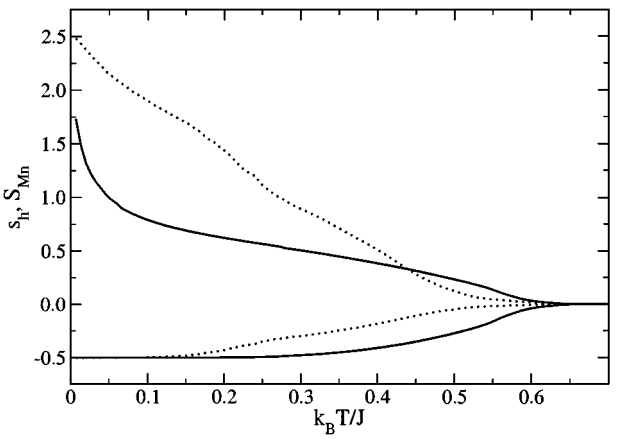


**Fig. 7.** Average magnetization of the Mn spin ($S_{Mn} > 0$) and of the charge carrier spins ($s_h < 0$) as a function of temperature, in a III–V DMS. Curves correspond to $x = 0.0093$ and $p = 10$ (full line) and 30% (dotted line), and were obtained using the mean-field approximation [21].

magnetization does not reach its saturation value until very low temperatures. Concurrently, the specific heat curves also exhibit a peak at temperatures much lower than the critical temperature, reflecting the entropy of the disordered spins present in the system down to these low temperatures [21].

By looking at the magnetization profile around the $T_C$, long-range ferromagnetism in the disordered sample of III–V DMS is seen to appear when a percolated cluster of polarized Mn spins is formed. However, unlike in the spin-only model based on isolated hydrogenic centers used for II–VI DMS in the previous section, the holes are *delocalized* within this cluster for the parameters appropriate for the III–V based DMS. Since the holes can more effectively minimize their kinetic energy when maintaining the direction of their spin during hopping, this delocalization of the holes within the percolated cluster provides a very effective mechanism for alignment of all Mn spins within the cluster in the same direction. This kinetic-induced alignment mechanism is much more effective than mechanisms of alignment of nearby BMPs in insulating II–VI DMS, suggesting higher critical temperatures in this case. Other reasons for enhancement of critical temperatures in III–V DMS include the peaking of the impurity wave-functions at the Mn sites in this case where Mn is also the dopant, and the ability of carriers in the compensated case to choose states with wave-functions peaked in the regions with higher-than-average Mn concentrations—the higher probability of finding the holes in these regions leads

to enhanced effective interactions with the Mn spins. When all these factors are included, we find indeed that the striking differences in critical temperatures, by two orders of magnitude, in the two systems can be comfortably explained, at least within MFA.

### 4.4. Effect of Disorder

Within the MFA, positional disorder in the Mn spins for III–V DMS leads to a significant increase of the critical temperature. Mn are the charged dopants in this case, so the situation again appears to be similar to that in II–VI DMS. Typical magnetization curves obtained using MFA are shown in Fig. 8, for a doping $x = 0.0093$ and $p = 10\%$. In order of increasing $T_C$, the four curves correspond to increasing disorder in the positions of the Mn impurities. We start with a fully ordered, simple cubic superlattice of Mn impurities inside the host semiconductor (for this concentration, the superlattice constant is equal to three lattice constants of the underlying Ga FCC sublattice). The corresponding average spins of the Mn and charge carriers are shown by dashed lines in Fig. 8. Then, we introduce positional disorder of the Mn ions on the underlying Ga FCC sublattice in varying amounts—(i) low-disorder where Mn spins are randomly placed on any of the nearest-neighbor sites of the original superlattice sites; (ii) moderate disorder—where the Mn spins are allowed to occupy any sites on the Ga sublattice, as long as the distance between any two Mn is larger than two lattice constants; and (iii) completely random positions of the Mn spins on the Ga FCC sublattice of the host semiconductor.

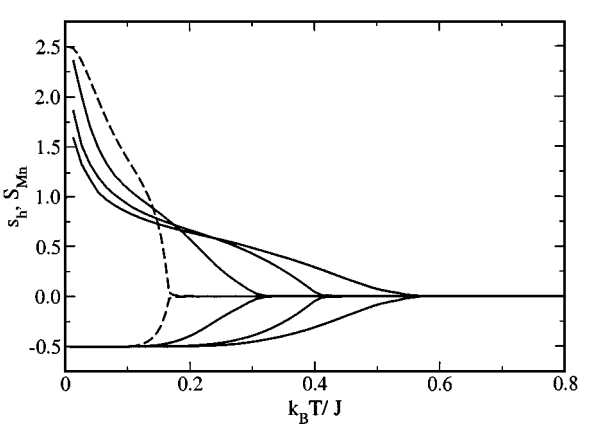


**Fig. 8.** The average Mn spin $S_{Mn}$ and average spin per hole $s_h$ for doping concentration $x = 0.00926$ and $p = 10\%$. In increasing order of $T_C$, the curves correspond to ordered, weakly disordered, moderately disordered, and completely random distributions of Mn (see text).

In a fully ordered III–V DMS, below $T_C$ each Mn spin is equally polarized, since translational invariance implies that the holes are equally distributed among the various Mn sites and therefore create the same effective magnetic field for each Mn spin. (In this respect the ordered lattice for III–V is different from the situation encountered for the ordered superlattice of charged dopants in the II–VI DMS. In the II–VI, below $T_C$ the Mn spins inside the BMPs are strongly polarized, while the Mn spins outside the BMPs are practically unpolarized.) The reason why $T_C$ is larger in a disordered III–V DMS than an ordered one, is that the hole wave-functions are pulled-in the regions with higher-than-average Mn concentrations, where they can more effectively minimize their total energy. The increased probability of finding the holes in this smaller volume occupied by the cluster leads to effectively larger couplings $J_{eff}$ of the Mn spins in the cluster [21], and therefore increased critical temperatures. In other words, in the disordered III–V DMS the holes only need to polarize a smaller fraction of the Mn spins in the system and get polarized in their own term. In an ordered Mn sample, the holes polarize equally *all* the Mn spins in the system, and this can only happen at rather low temperatures, given the small number of holes as compared with the number of Mn spins. While MFA shows a strong dependence of $T_C$ on disorder, this is likely to be modified once fluctuation effects left out in MFA are included, as in a MC simulation.

The unusual shape of the magnetization curves is a consequence of the relatively small number of charge carriers as compared to the number of Mn spins. In a disordered system, we can identify two types of Mn spins: strongly interacting Mn spins from the percolated cluster, which polarize at high temperatures and lead to the ferromagnetic transition at $T_C$, and weakly interacting Mn spins from the regions outside the percolated cluster. Since these outside regions have low-hole density in our model, the effective coupling of their Mn spins (which is proportional to the probability of finding holes nearby) is rather small. Consequently, these spins do not polarize unless the temperature is comparable in size to their effective coupling. We have used this picture to obtain a simplified but fairly accurate description of the magnetic and thermodynamic properties of the DMS based on a two-component model [24]. We start from a histogram of the effective couplings $J_{eff}$ of all the Mn

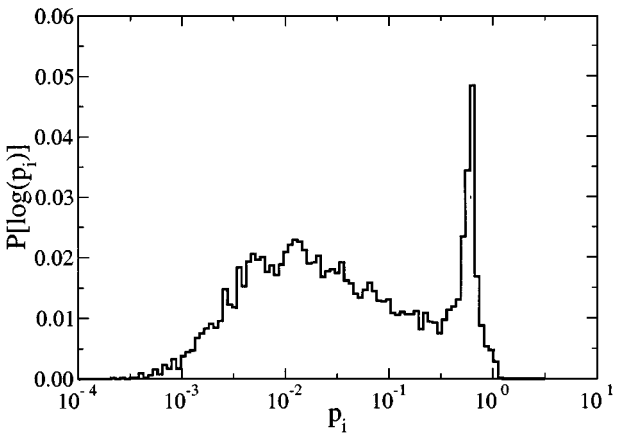


**Fig. 9.** Histogram of effective couplings $p_i = J_{\rm eff}(i)/J$ of different Mn spins at $k_{\rm B}T/J = 0.01$, for $x = 0.01$ and relative hole to Mn concentration $p = 10\%$. This distribution was found using Monte Carlo simulations [22].

spins, obtained by averaging over many realizations of disorder. Such a histogram of $J_{\rm eff}/J$ obtained using MC simulations for $x = 0.01$ and $p = 10\%$ is shown in Fig. 9. As can be seen, it is a very wide distribution, from very large $J_{\rm eff} \sim J$ for strongly interacting Mn spins, to extremely small $J_{\rm eff}/J \sim 10^{-3}$ values for weakly interacting Mn spins. Histograms obtained within the MFA have very similar shapes, except that their width is even larger [21].

For such wide distributions, at any given temperature $k_{\rm B}T$, we divide the spins into weakly/strongly interacting categories, depending of whether their effective coupling $J_{\rm eff}$ is smaller/larger than $\gamma k_{\rm B}T$. Then, we replace the complex distribution of couplings shown in Fig. 9 by two $\delta$-functions representing the two spin components. The values of the nominal couplings $J_1$ and $J_2$ of the weakly/strongly interacting spin components are simply the average of all the couplings of weakly/strongly interacting spins. The constant $\gamma$ is found from a fit of, for instance, the magnetization curve provided by this simplified model. Other thermodynamic quantities, such as susceptibility and specific heat are then shown to be quite well described by this simple model [24]. In contrast, we have verified that replacing all the couplings by a *single* coupling corresponding to the average over the entire distribution leads to curves very different than the ones obtained with the original distribution. We believe this simplified model could provide a simple tool for interpretation of experimental curves. So far, most attempts have been to try to fit the magnetization curves (for instance) with only one coupling. While this may recapture part of the curve near and below $T_{\rm C}$ [9], it turns out that it only accounts for a rather small percentage of the total number of Mn spins expected to be in the system. This suggests that a second component is missing. In fact, fits in terms of two components, one ferromagnetic and one paramagnetic, have already been performed in order to explain the shapes of the measured $M(H, T)$ curves [25].

In a conventional ferromagnet, an external magnetic field will lead to a fast increase of the magnetization from its value in the absence of the field, to the saturation value $M_0 = Ng\mu_{\rm B}S$, where $N$ is the concentration of spins $S$ in the system. A hysteresis curve associated with the existence of ferromagnetism below $T_{\rm C}$ is also observed. In III–V DMS samples, the hysteresis curves are clearly observed as well. However, even at rather large fields $H$, $M(H)$ does not saturate, but continues to increase with increasing magnetic field. This feature has been attributed to a "paramagnetic" component [25], and it obviously corresponds to the weakly interacting component of nearly free spins of our simplified two-component model. In fact, we have generated $M(H, T)$ curves within the MFA, and these features are clearly present (see Fig. 10), in qualitative agreement with measurements.

### 4.5. Effect of Other Interactions

We have investigated in detail the effect of the on-site disorder term $u(i)$ and of the on-site Coulomb repulsion $U$ elsewhere [21]. The on-site disorder is

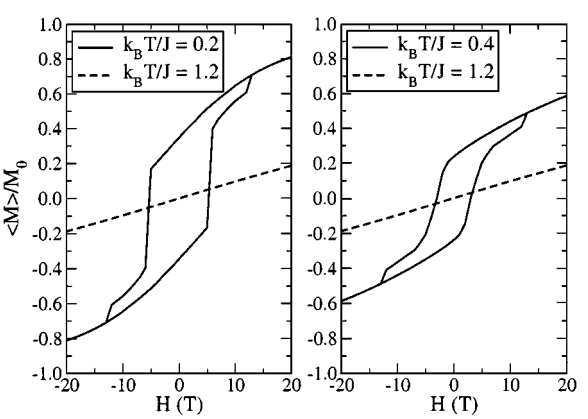


**Fig. 10.** Hysteresis curves obtained within the mean-field approximation for *one disorder realization* corresponding to a Mn concentration $x = 0.03$ and hole to Mn ratio $p = 10\%$ (corresponding to a critical temperature $k_{\rm B}T_{\rm C}/J = 0.85$). Averages over several disorder realizations are needed to obtain smooth curves.

due to the Coulomb potential created by the charge impurities responsible for compensation (such as $As^{++}$ antisites). We have considered two extreme possibilities. In the first case, we assume that these potentials are completely uncorrelated, and model them by choosing random values for $u(i)$ within an interval $[-W, W]$. The estimate $W \approx 1$ Ry is obtained following standard considerations for doped semiconductors [26]. In the second case, we attempt a simple modeling of the effect of As antisites. We choose random positions for these As defects on the Ga sublattice and identify their two nearest neighbor Mn sites. Each such As impurity has an effective charge $+2e$, and therefore will contribute an on-site Coulomb potential $+2e^2/\epsilon r$ at a Mn impurity site which is at a distance $r$ from it. However, since the Mn ions also have effective ionic charge $-e$, the As potential is screened (partially compensated) by the potential of the Mn impurities nearby it. Therefore, we assume that each As antisite only contributes to the on-site potential $u(i)$ of its two nearest Mn neighbors, with the contribution to the other Mn sites being screened out by the contribution of these two nearest Mn sites. The presence of the charged impurities responsible for compensation increases the amount of disorder (inhomogeneity) in the system, since the holes will avoid the regions were these defects are located. Thus, one might assume that $u(i) \neq 0$ will lead to a further increase of $T_C$. However, in fact we find a decrease of $T_C$ for these models of compensation, especially for the second model [21]. This is a consequence of the fact that due to the presence of nearby As antisites, holes now avoid some Mn sites that would otherwise be part of dense clusters. Thus, the system effectively moves toward the more homogeneous regime, with lower $T_C$. An opposite effect is provided by the on-site electron–electron Coulomb repulsion, the presence of which was found to lead to an increase of $T_C$, since it aids in the splitting of the up and down spin bands, favoring spin polarization at higher temperatures [21].

A quantitative determination of the effects of these types of interactions will have to wait until more details are known about the compensation processes. A theory that properly and self-consistently describes the screening processes is also necessary.

## 5. CONCLUDING REMARKS

In this paper, we have discussed the behavior of a model of DMS in the low density regime, based on a simple tight-binding hydrogenic model of the impurity band. Such a model takes into account, at the very outset, the inherent disorder present in the experimental system, namely the random position of the dopants. Other models [3] start from an electron gas exhibiting the translational symmetry of the host lattice and ignore the disorder of the alloy system. While the latter may be the appropriate starting point for the high carrier density regime, it does not allow for a metal-insulator transition, and consequently misses the unusual transport and magnetic behavior associated even with metallic systems in the vicinity of such a transition. In contrast, our model starts from the low density insulating side, and at least for conventional doped semiconductors, has been found to be applicable to densities up to a factor of 3 above the metal-insulator transition [27].

For the case of II–VI DMS, we have restricted ourselves to low densities corresponding to the insulating phase, for the case of a half-filled band i.e., no compensation. In this limit, a spin-only description of the bound carriers is appropriate. (We note, however, that such a spin-only description has been very successful for the low-temperature thermodynamic and magnetic properties in conventional doped semiconductors, both uncompensated and compensated, for densities up to the metal-insulator transition [5] and even somewhat into the metallic phase [28,29] provided an itinerant Fermi liquid-like second component is added to the description of these highly disordered systems.) For III–V DMS, where large compensation is found to be experimentally present, presumably due to antisite defects, we have adopted a full fermionic description of the carriers. Such a model allows for both an insulating and a metallic phase. However, as explained in the body of the paper, the model we have studied is simplified, and neglects several terms in the full many-body Hamiltonian describing these complicated materials.

Despite the rather different model descriptions (spin vs. fermion) for the two cases, as well as methods of solution (Monte Carlo vs. mean-field approach), we find a remarkable similarity in the qualitative predictions concerning the magnetic and thermodynamic properties. Most striking are the unusual magnetization curves $M(T)$, with linear to concave upwards shape over much of the ferromagnetic region, in striking contrast to conventional uniform ferromagnets. This appears to be a combined result of low carrier density and strong disorder. As a consequence, the ferromagnetic transition has percolation like characteristics, with only a small fraction

of the material carrying the bulk of the ferromagnetism around $T_C$. The remaining portion of the material orders gradually as the temperature is lowered, and unlike in most conventional ferromagnets, saturation magnetization is not reached until well below $T_C$. Such an inhomogeneous magnetization results in unusual susceptibility and specific heat in the low temperature ordered phase, and would imply substantial inhomogeneities in the local field at Mn sites, which could be probed, e.g., by NMR measurements. Unusual hysteresis curves in $M(H)$ below $T_C$ are also implied, with saturation occurring well beyond where the loops close. We have checked for the case of the III–V DMS that within a simple impurity band description, these effects are robust [21]. However, as the carrier density is increased (by reducing the compensation, or raising the Mn concentration), the anomalous shape of $M(T)$ becomes less prominent: $M(T)$ assumes the convex upward shape of conventional uniform ferromagnets, and the ensuing unusual properties discussed above gradually fade away.

In contrast to the qualitative shape of the magnetization curves and the ensuing thermodynamic and magnetic behavior, the actual transition temperatures of the two systems are known to be rather different (from a few degrees kelvin [8] for the II–VI DMS, to several hundreds [9,16,30,31] for the III–V DMS). Certainly one reason for this difference is the increased weight of the hole wave-function at the cation (II/III) site where the Mn spin resides in the III–V semiconductors relative to the II–VI semiconductors, as may be seen from a tight-binding description of valence bands [32] of zinc-blende structure semiconductors. However, an additional reason within an impurity band description of carriers, is that in III–V DMS the Mn sites are centers of the impurity wavefunctions, while for II–VI DMS, the carrier impurity sites are distinct from the Mn. Consequently, the Mn sites see a lower amplitude of the carrier wavefunction, and thus a lower effective exchange coupling in the II–VI. This peaking of the impurity wavefunction at the Mn site in the III–V based DMS, leads to a further enhancement of their $T_C$ vis-a-vis the II–VI based DMS.

For both the II–VI and the III–V DMS, we find that $T_C$ is enhanced by disorder. This can be understood by recognizing that in a heavily disordered system, nature is able to create global ordering by finding the tortuous percolative pathway necessary when the average coordination number is much below that of any uniform lattice [26]. In III–V, the large compensation adds an additional degree of freedom to the carriers, in the choice of amplitudes on different sites, which again leads to wide variation in the effective fields at different sites, and implies a percolative aspect to the magnetic ordering transition. In mean field, we find the enhancement of $T_C$ to be quite large; however, preliminary MC results suggest lower effects of disorder on $T_C$ than given by the mean-field approach [22].

Disorder effects on the electronic wave-functions will lead to significant transport anomalies, especially near the metal-insulator transition, as has been seen experimentally [9]. It will also likely affect the nature and amount of magnetic scattering of carriers injected into the system. While the naive expectation is that disorder should increase spin-flip scattering, it may be significantly reduced for carriers near the Fermi level. This is because we find that these states have large amplitudes along the percolating backbone of the system, where the Mn moments are magnetized well above the average global magnetization. In this regime, many standard models devised for translationally invariant systems (e.g., relationship of anomalous Hall effect to bulk magnetization) may not be applicable, and such interpretations should be used with care.

One other approximation inherent in our work is the assumption that electron and hole doping give rise to Hamiltonians that are qualitatively similar, though quantitatively different (holes have angular momentum 3/2, while electrons have spin 1/2). This is what is found for free holes [33]: although the more complicated anisotropic wave-functions for holes lead to quantitative differences, qualitatively the results are similar, in that both systems lead to ferromagnetic ordering. Recently, however, since the Spintronics 2001 conference, it has been proposed [34] that spin–orbit coupling can lead to effective spin–spin couplings that are *anisotropic* in spin space, and the positional disorder effectively leads to random anisotropy. This could lead to frustration effects not present in our model, and if true, would need to be put in for hole doped systems to achieve full understanding of magnetic ordering and carrier transport in DMS systems.

Finally, we discuss the applicability of our results to actual III–V DMS in the regime of large $T_C$. While our model is based on the insulating, low density limit, how many of its features persist into the metallic phase at higher densities and temperatures, is dependent on the nature of the filled electronic states at temperatures $T_C$ and below. In the model we have studied, the host valence band is completely neglected, and its inclusion is not expected to lead to qualitative changes,

because it lies several hundred meV above the Fermi level. However, this is a consequence of an impurity band with a density of states that is characteristic of a bandwidth of order hundred meV also. Should the impurity band become much broader in the actual system due to effects we have left out, it will likely merge into the host valence band, and the states will be strongly mixed. Nevertheless, the occupied states for small filling (low Mn density and large compensation) would have significant effects of disorder. This, in turn, implies that the anomalous behavior exhibited by our model would be present, but with lower magnitude than shown by our calculations. The clearest signature of these would likely come from local probes, which would be able to determine the distribution of *local* fields, and hence *local* density of states at various sites. Such input into phenomenological models should provide a fruitful avenue for a more in-depth study of the fascinating world of real DMS, which offer both a significant promise in terms of their applications in spintronics, and a challenge in terms of their fundamental understanding.

## ACKNOWLEDGMENTS

This research was supported by NSF DMR-9809483. R.N.B. acknowledges the hospitality of the Aspen Center of Physics during their Spins in Nanostructures workshop, when this presentation for the Spintronics 2001 conference was organized. M.B. was supported in part by a Postdoctoral Fellowship from the Natural Sciences and Engineering Research Council of Canada.

## REFERENCES

1. H. R. Ott, in *More Is Different—Fifty Years of Condensed Matter Physics*, N. P. Ong and R. N. Bhatt, eds. (Princeton University Press, Princeton, NJ, 2001).
2. J. A. Mydosh, *Spin Glasses: An Experimental Introduction* (Taylor and Francis, London, 1993).
3. T. Dietl, A. Haury, and Y. M. d'Aubigné, *Phys. Rev. B* **55,** R3347 (1997); M. Takahashi, *Phys. Rev. B* **56,** 7389 (1997); T. Jungwirth, W. A. Atkinson, B. H. Lee, and A. H. MacDonald, *Phys. Rev. B* **59,** 9818 (1999); T. Dietl, H. Ohno, F. Matsukura, J. Cibert, and D. Ferrand, *Science* **287,** 1019 (2000); J. König, H.-H. Lin, and A. H. MacDonald, *Phys. Rev. Lett.* **84,** 5628 (2000); A. Chattopadhyay, S. Das Sarma, and A. J. Millis, *Phys. Rev. Lett.* **87,** 227202 (2001).
4. R. N. Bhatt and P. A. Lee, *Phys. Rev. Lett.* **48,** 344 (1982).
5. R. N. Bhatt, *Physica Scripta T* **14,** 7 (1986).
6. P. A. Wolff, R. N. Bhatt, and A. C. Durst, *J. Appl. Phys.* **79**, 5196 (1996); A. C. Durst, R. N. Bhatt, and P. A. Wolff, cond-mat/0111497.
7. D. E. Angelescu and R. N. Bhatt, cond-mat/0012279.
8. J. K. Furdyna and J. Kossut, *Semiconductors and Semimetals, Vol. 25* (Academic Press, New York, 1988).
9. H. Ohno, *J. Magn. Magn. Mat.* **200,** 110 (1999).
10. H. Eugene Stanely, *Introduction to Phase Transitions and Critical Phenomena* (Oxford University Press, New York, 1971).
11. M. Sawicki, L. Van Khoi, L. Hansen, D. Ferrand, L. W. Molenkamp, A. Waag, and T. Dietl, *Phys. Status Solidy* (in press).
12. S. Oseroff and P. H. Keesom, in *Diluted Magnetic Semiconductors*, J. K. Furdyna and J. Kossut, eds. (Academic Press, New York, 1988).
13. K. Andres, R. N. Bhatt, P. Goalwin, T. M. Rice, and R. E. Walstedt, *Phys. Rev. B* **24,** 244 (1981).
14. R. N. Bhatt and X. Wan, *Int. J. Mod. Phys. C* **10,** 1459 (1999); X. Wan and R. N. Bhatt, cond-mat/0009161.
15. X. Wan and R. N. Bhatt, unpublished.
16. A. Van Esch, L. Van Bockstal, J. De Boeck, G. Verbanck, A. S. van Steenbergen, P. J. Wellmann, G. Grietens, R. Bogaerts, F. Herlach, and G. Borghs, *Phys. Rev. B* **56,** 13103 (1997).
17. S. Katsumoto, A. Oiwa, Y. Iye, H. Ohno, F. Matsukura, A. Shen, and Y. Sugawara, *Phys. Status Solidy B* **205,** 115 (1998).
18. A. K. Bhattacharjee and C. B. á la Guillaume, *Solid State Comm.* **113,** 17 (2000).
19. M. Berciu and R. N. Bhatt, *Phys. Rev. Lett.* **87,** 107203 (2001).
20. R. N. Bhatt, *Phys. Rev. B.* **24,** 3630 (1981).
21. M. Berciu and R. N. Bhatt, cond-mat/0111045.
22. M. P. Kennett, M. Berciu, and R. N. Bhatt, unpublished; R. N. Bhatt, X. Wan, M. P. Kennett, and M. Berciu, *Comp. Phys. Comm.* (in press).
23. B. Beschoten, P. A. Crowell, I. Malajovich, D. D. Awschalom, F. Matsukura, A. Shen, and H. Ohno, *Phys. Rev. Lett.* **83,** 3073 (1999).
24. M. P. Kennett, M. Berciu, and R. N. Bhatt, cond-mat/0102315.
25. A. Oiwa, S. Katsumoto, A. Endo, M. Hirasawa, Y. Iye, H. Ohno, F. Matsukura, A. Shen, and Y. Sugawara, *Solid State Comm.* **103,** 209 (1997).
26. B. I. Shklovskii and A. L. Efros, *Electronic Properties of Doped Semiconductors* (Springer, Berlin, 1984).
27. N. F. Mott, *Metal Insulator Transitions* (Taylor and Francis, London, 1990); R. F. Millikan, T. F. Rosenbaum, R. N. Bhatt, and G. A. Thomas, in *Electron–Electron Interactions in Disordered Systems*, A. L. Efros and M. Pollak, eds. (Elsevier, Amsterdam, 1985), pp. 231–286.
28. R. N. Bhatt, M. A. Paalanen, and S. Sachdev, *J. de Physique Colloq. C* **8,** 1179 (1988).
29. M. J. Hirsch, D. F. Holcomb, R. N. Bhatt, and M. A. Paalanen, *Phys. Rev. Lett.* **68,** 1481 (1992).
30. N. Theodoropoulos, A. F. Hebard, M. E. Overberg, C. R. Abernathy, S. J. Pearton, S. N. G. Chu, and R. G. Wilson, *Appl. Phys. Lett.* **78,** 3475 (2001).
31. S. Sonoda, S. Shimizu, T. Sasaki, Y. Yamamoto, and H. Hori, cond-mat/0108159.
32. D. J. Chadi and R. M. Martin, *Solid State Commun.* **19,** 643 (1976); D. J. Chadi, *Phys. Rev. B* **19,** 2074, Table I (1979).
33. J. Schliemann, J. Konig, and A. H. MacDonald, *Phys. Rev. B* **64,** 165201 (2001).
34. G. Zarand and B. Janko, cond-mat/0108477.